Efficient Design of FMT Systems for Digital Subscriber Lines*†

Bahram Borna and Timothy N. Davidson

Technical Report,
Department of Electrical and Computer Engineering,
McMaster University,
Hamilton, Ontario, L8S 4K1, Canada.
Email: davidson@mcmaster.ca

September 2004
Revised July 2005

Abstract

Filtered multitone (FMT) modulation is a multicarrier modulation scheme which is implemented using a modulated filter bank structure and is a candidate for very high-speed digital subscriber line (VDSL) technology. In this paper we propose an efficient design method for the prototype filter in the FMT filter bank. Our method allows efficient evaluation of the inherent trade-off between the subchannel spectral containment provided by the prototype filter and the intersymbol interference (ISI) that the filter generates. An appropriate operating point on this trade-off curve is then identified by computing the achievable bit rate for FMT systems with prototype filters which lie on the curve. Our numerical results indicate that careful exploration of the filter design trade-off results in a significant gain in the achievable bit rate. Furthermore, the insight gained from this design can be transferred to the choice of the optimal number of subchannels. Finally, since the presence of ISI in FMT subchannels renders the conventional water-filling power loading algorithm suboptimal, we propose an efficient power loading algorithm for FMT that enables higher achievable bit rates.

*This work was supported in part by the Natural Sciences and Engineering Research Council of Canada. The work of the second author is also supported in part by the Canada Research Chairs program.

†A preliminary version of Sections 3 and 4 of this report appeared in the *Proceedings of the IEEE International Conference on Communications*, Paris, June 2004, and a condensed version has been submitted to the *IEEE Transactions on Communications*.

1 Introduction

Very high speed digital subscriber line (VDSL) is the moniker for the next generation of digital subscriber line (DSL) technology. An objective of VDSL system design is to be capable of delivering a variety of broadband services for typical line lengths of up to 2000 meters [1]. However, the DSL environment is a rather hostile one, especially at the higher end of the spectral band proposed for VDSL. In addition to thermal noise, DSL communication systems have to mitigate other interferences, including far-end crosstalk (FEXT), near-end crosstalk (NEXT), echo, narrowband radio interference, and impulsive noise [2]. Of course, the frequency selectivity of the DSL channel also results in severe inter-symbol-interference (ISI). To combat ISI, multicarrier modulation schemes are often employed in DSL systems. In particular, a discrete multitone (DMT) modulation scheme that employs the "Zipper" frequency division duplexing [3] is one of the candidates for VDSL. Filtered multitone (FMT) modulation [4, 5] is an alternative candidate for VDSL that offers some advantages over DMT [4]. In particular, FMT modulation provides a high level of subchannel spectral containment and thereby reduces the impact of echo, self-NEXT, narrowband interference, and regulatory spectral masks. Furthermore, FMT modulation does not require synchronization of the upstream and downstream transmissions on a given link [4]. Indeed, it has been shown [4] that FMT-based VDSL systems offer the potential for larger achievable bit rates than DMT-based VDSL systems.

FMT modulation is implemented using a modulated filter bank structure. The prototype filter for this filter bank is a key design parameter, and some preliminary design methods have been proposed [4–6][1]. In this paper, we develop a more comprehensive approach for the design of prototype filter and demonstrate the engineering insight that this method generates. The proposed filter design approach begins with the derivation of design criteria which lead to increased subchannel signal to interference and noise ratios (SINRs) at the receiver. The design of the filter requires a compromise between these criteria and therefore there is a trade-off to be explored. In order to explore the trade-off we formally cast the design problem as an optimization problem. As we will show, the direct formulation of that optimization problem is non-convex in the design variables and hence the exploration of the trade-off is hindered by the intricacies of dealing with the potential for locally optimal solutions. However, we will show that the design problem can be precisely transformed into a convex optimization problem from which a globally optimal solution can be found. The convex formulation allows us to efficiently compute the inherent trade-off between the competing design criteria. Further numerical analysis then allows us to determine points on the trade-off curve that provide a large achievable bit rate. While the focus of our design examples will be on VDSL systems, FMT is also attracting attention as a candidate technology for certain wireless communication applications [8, 9]. The design methods developed herein remain valid for

[1] The design of FMT systems with different prototype filters at the transmitter and receiver has also been considered [7].

those applications.

To demonstrate the versatility of the proposed prototype filter design technique, we also use it to evaluate the trade-offs between intersubchannel interference (ICI), intersymbol interference (ISI), and transceiver complexity that arise when choosing the number of subchannels in an FMT system. These evaluations provide important guidelines for the design of FMT systems.

One of the key differences between DMT and FMT systems is the high level of subchannel spectral containment provided by FMT. However, this spectral containment is achieved at the cost of ISI within each subchannel. (The trade-off between these criteria is a key component of our design approach.) The presence of ISI means that the conventional water-filling power loading algorithms developed for DMT systems yield suboptimal results unless a relatively high complexity decision feedback equalizer (DFE) is used in each subchannel of the receiver. For applications in which only simple DFEs are employed, we propose an efficient power loading algorithm that iteratively accounts for the residual ISI and hence enables higher achievable bit rates than conventional water-filling.

2 System description

The block diagram of an M-channel FMT system in which the upstream and downstream subchannels are interleaved is shown in Fig. 1. The filter bank is constructed from a single real finite impulse response (FIR) prototype filter with impulse response $h[n]$ and frequency response $H(e^{j\omega})$. The transmission filter for each subchannel is a frequency-shifted version of the prototype filter and the first step performed by the receiver is matched filtering of each subchannel (the superscript * denotes complex conjugation). The separation between the centre frequencies of adjacent subchannels is equal to $2\pi/M$, where M is the number of subchannels. For ease of exposition, in Fig. 1 we have considered an equal number of subchannels for upstream and downstream directions (symmetric communication) arranged in a "zipper-like" duplexing pattern [3]. However, the discussion in this article is applicable to other carrier arrangements as well (e.g., asymmetric communication).

We now provide a brief review of the operation of this system in the downstream direction (the upstream direction is analogous). Sequences of complex-valued symbols $x_i[n]$ are chosen from not necessarily identical constellations at the symbol rate $1/T$. These symbols are then processed using an efficient FFT-based polyphase implementation [4,11] of the upsampling and filtering operations illustrated in Fig 1. The transmit signal is then formed by adding all the filtered sequences and applying digital to analog conversion (D/A) at a sampling rate of $1/T_s = N/T$. This signal is then transmitted over the wire pair channel (with impulse response $h_c(t)$) that forms the subscriber line. The received signal is sampled every T_s seconds and is passed through (an efficient implementation of) a bank of subchannel matched filters and then downsampled by a factor of N. Since the combined frequency response of the subchannel filters and the channel is not necessarily flat over the bandwidth of the subchannels, intersymbol interference (ISI) is present at the subchannel outputs. In order to mitigate the effects of this ISI without incurring large computational expense, FMT

schemes typically incorporate a symbol-rate decision feedback equalizer (DFE) into the detector in each subchannel [4, 9, 10]. We focus our attention on such systems in this paper. Although not shown in Fig. 1, thermal noise is modeled as additive white Gaussian noise (AWGN) at the receiver input and colored interference from other sources is also considered at the receiver. The blocks marked by "H" in Fig. 1 are line hybrids [2], which are used to provide isolation between the transmitter and the near-end receiver and thereby suppress self-echo. The equivalent discrete-time channel impulse response for the concatenation of the D/A, the analog channel, and the A/D is denoted by $c[n]$.

The fundamental idea behind FMT modulation is subchannel separation via filtering. This enables effective detection of the transmitted symbols using a per-subchannel detector rather than joint detection. In order to provide sufficient subchannel separation with filters of reasonable complexity, redundant filter banks are usually employed; i.e., $N > M$. This results in a digital analogue of conventional frequency division multiple access techniques with guard bands. In the following section, we derive design criteria for the prototype filter of the filter bank which measure the degree of subchannel separation and the ISI induced by subchannel filters.

3 System analysis and filter design

To simplify the analysis of the system of Fig. 1 we assume that the input data sequences of different subchannels are uncorrelated and that the symbols for each input sequence are uncorrelated with each other; i.e.,

$$E\left\{x_i[n_1]x_\ell^*[n_2]\right\} = P_i\,\delta[i-\ell]\delta[n_1-n_2], \tag{1}$$

where $E\{\cdot\}$ denotes the statistical expectation operation, $\delta[\cdot]$ is the Kronecker delta, and P_i is the power of the ith input sequence $x_i[n]$. In the following analysis we will study the input-output equations for downstream communication. A similar analysis applies in the upstream case. For ease of exposition, the initial analysis in this section will be done in the absence of external noise/interference (including AWGN of the analog channel, echo, NEXT, and FEXT). Thus, the output signal for each subchannel will include only components due to the desired symbol, inter-symbol interference (ISI), and intersubchannel interference (ICI). Later, we will comment on the effects of external interference.

Let $\mathcal{A}$ denote the set of carrier indices used for downstream communication. (In Fig. 1, $\mathcal{A} = \{1, 3, \cdots, M-1\}$.) For the mth subchannel at the receiver, $m \in \mathcal{A}$, the signal at the input to the detector in Fig. 1 depends on the downstream input sequences through the following equation

$$y_m[n] = \sum_{i\in\mathcal{A}} x_i[n] \star f_{mi}[n]\ , \tag{2}$$

where i denotes the index of the subchannel at the transmitter, the symbol $\star$ denotes convolution,

and

$$f_{mi}[n] = g_{mi}[Nn] \ , \tag{3}$$

where

$$g_{mi}[n] = h_i[n] \star c[n] \star h_m^*[-n], \tag{4}$$

$h_i[n] = h[n]e^{j\omega_i n}$ is the inverse Fourier transform of $H(e^{j(\omega-\omega_i)})$, and for notational convenience we have allowed non-causal (matched) filtering at the receiver. For data symbols that satisfy (1), the power spectral density (PSD) of $y_m[n]$ can be written as

$$S_{y_m}(e^{j\omega}) = \sum_{i\in\mathcal{A}} P_i |F_{mi}(e^{j\omega})|^2 \tag{5}$$

$$= P_m |F_{mm}(e^{j\omega})|^2 + \sum_{\substack{i\in\mathcal{A} \\ i\neq m}} P_i |F_{mi}(e^{j\omega})|^2, \tag{6}$$

where $F_{mi}(e^{j\omega})$ is the Fourier transform of $f_{mi}[n]$. In (6), the first term on the right hand side is the PSD of the matched filtered signal from the mth transmitter, i.e., the component of $S_{y_m}(e^{j\omega})$ due to the desired symbol and the ISI. The second term is the PSD of the signals from other downstream subchannels at the mth subchannel output, i.e., the component of $S_{y_m}(e^{j\omega})$ due to ICI.

If we let $S_{\mathrm{ICI}}(e^{j\omega})$ denote the PSD of ICI, the power of ICI can be written as

$$P_{\mathrm{ICI}} = \frac{1}{2\pi}\int_0^{2\pi} S_{\mathrm{ICI}}(e^{j\omega})\, d\omega = \frac{1}{2\pi}\int_0^{2\pi} \sum_{\substack{i\in\mathcal{A} \\ i\neq m}} P_i |F_{mi}(e^{j\omega})|^2 \, d\omega. \tag{7}$$

In Appendix A, we show that P_{ICI} can be bounded by

$$P_{\mathrm{ICI}} \leq P_I U_c^2 (U_p^2 E_{sb} + U_{sb}^2 E_h + U_{sb}^2 E_{sb}), \tag{8}$$

where $P_I = \max_{i\in\mathcal{A}}\{P_i\}$, E_{sb} is the stopband energy of the prototype filter,

$$E_{sb} = \frac{1}{2\pi}\int_{\frac{\pi}{M}}^{2\pi-\frac{\pi}{M}} |H(e^{j\omega})|^2 \, d\omega, \tag{9}$$

E_h is the energy of the prototype filter, $E_h = \frac{1}{2\pi}\int_0^{2\pi} |H(e^{j\omega})|^2 \, d\omega$, and U_p and U_{sb} are the maximum values of $|H(e^{j\omega})|$ in the passband ($\omega \in (-\pi/m, \pi/M]$), and stopband ($\omega \in [\pi/M, 2\pi - \pi/M]$), respectively. In (8), U_c is an upper bound for $|C(e^{j\omega})|, \ \forall\omega$.

The value of (8) is that it provides an upper bound on the power of the ICI in terms of standard characteristics of the prototype filter. A similar analysis can be performed for NEXT and echo, since both of these effects can be modeled in a similar way but with a different channel model replacing $c[n]$. Thus, corresponding upper bounds hold for the power of NEXT and echo, but with

different models for $c[n]$.

Another performance measure that we consider in filter design is ISI. From (2), we have that the power of the desired signal component at the input to the detector is $P_m|f_{mm}[d]|^2$, where the delay d is typically chosen to be $d = \arg\max_n |f_{mm}[n]|$. The power of the ISI component is

$$P_{\text{ISI}} = P_m \sum_{n \neq d} |f_{mm}[n]|^2. \tag{10}$$

In the FMT system of Fig. 1, ISI is introduced both by the filter bank and the channel. To study the ISI which is introduced by the filter bank alone, we assume that the frequency response of the channel is ideal over the subchannel bandwidth. In that case, the appropriate delay is $d = 0$ and the signal to ISI power ratio is

$$\frac{\text{Signal power}}{\text{ISI power}} = \frac{E_h^2}{\sum_{n\neq 0}(\sum_k h[k]h[k-Nn])^2}\ , \tag{11}$$

where the denominator is obtained by substituting (3) and (4) into (10). Combining equations (8) and (11) we obtain the following design criteria for the prototype filter of the filter bank in Fig. 1:

1. Small values of the stopband energy, E_{sb}, the maximum stopband level, U_{sb}, and the maximum passband level, U_p, of the prototype filter will guarantee that the power of the ICI, NEXT and echo at the input to the detector are small.

2. When the energy of the prototype filter (E_h) is normalized, small values of the ISI factor $\sum_{n,n\neq 0} (\sum_k h[k]h[k-Nn])^2$, will guarantee that the power of ISI at the input to the detector is small.

Therefore, a natural design problem for the prototype filter would be to minimize the stopband energy of the filter, subject to upper bounds on the stopband level, the passband level, and the ISI power when the filter energy is normalized. That is,

$$\begin{aligned}
\text{minimize} \quad & \frac{1}{2\pi}\int_{\pi/M}^{2\pi-\pi/M} |H(e^{j\omega})|^2\, d\omega && \text{(12a)}\\
\text{subject to} \quad & |H(e^{j\omega})| \leq t_{sb}\,, \quad \frac{\pi}{M} \leq \omega \leq \pi\,, && \text{(12b)}\\
& |H(e^{j\omega})| \leq t_p\,, \quad \forall\omega\,, && \text{(12c)}\\
& \sum_{n,n\neq 0} \left(\sum_k h[k]h[k-Nn]\right)^2 \leq t_d^2\,, && \text{(12d)}\\
& \sum_k (h[k])^2 = E_h\,, && \text{(12e)}
\end{aligned}$$

where t_{sb}, t_p, and t_d^2 are positive real numbers that constrain the stopband level, passband level and

ISI power, respectively. In (12e), E_h is a positive real number to which the energy of the prototype filter is normalized.

Unfortunately, the constraint in (12d) is not convex, and hence algorithms for solving (12) are complicated by the need to deal with the intricacies of potential local minima. However, by using the autocorrelation function of $h[n]$ as the design variable, the problem in (12) can be precisely transformed [12] into the following convex optimization problem which can be efficiently solved for a globally optimal solution. In order to state the convex problem explicitly, we let L denote the length of the prototype filter and $r_h[n]$ denote the autocorrelation function $r_h[n] = \sum_\ell h[\ell]h[-n+\ell]$. We also let $R_h(e^{j\omega})$ denote the Fourier transform of $r_h[n]$, and define $b[0] = 1 - 1/M$ and $b[n] = -2/(\pi n)\sin(\pi n/M)$, $n = 1, 2, \cdots, L-1$. The problem in (12) can then be precisely transformed into the following convex optimization problem

$$\begin{aligned}
\text{minimize} \quad & \sum_{n=0}^{L-1} r_h[n]b[n] && \text{(13a)}\\
\text{subject to} \quad & R_h(e^{j\omega}) \le t_{sb}^2\,, \quad \frac{\pi}{M} \le \omega \le \pi\,, && \text{(13b)}\\
& R_h(e^{j\omega}) \le t_p^2\,, \quad \forall\omega\,, && \text{(13c)}\\
& \sum_{n\ge 1} r_h^2[Nn] \le \frac{t_d^2}{2}\,, && \text{(13d)}\\
& r_h[0] = E_h\,, && \text{(13e)}\\
& R_h(e^{j\omega}) \ge 0\,, \quad \forall\omega\,. && \text{(13f)}
\end{aligned}$$

While the problem in (13) is convex, equations (13b), (13c) and (13f) generate an infinite number of constraints (equations (12b) and (12c) also generate an infinite number of constraints). These constraints can be approximated by discretization or precisely enforced using linear matrix inequalities [13]. Once formulated in one of those forms, the problem in (13) can be efficiently solved for the optimal $r_h[n]$ using general purpose implementations of interior point methods, such as [14]. We can then extract a corresponding $h[n]$ using standard spectral factorization techniques [15, 16]. As we will demonstrate below, the convexity of the transformed optimization problem in (13) allows effective evaluation of the trade-off between subchannel separation and the ISI induced by the filter bank in an FMT system.

4 Numerical results

In this section we present numerical results for an FMT system with $M = 32$ subchannels, an up/down-sampling factor of $N = 36$ (for an excess bandwidth of 12.5%), and a prototype filter of length $L = 320$. For different values of the ISI factor, t_d, we found a prototype filter with minimum

stopband energy by solving the convex optimization problem in (13). The resulting inherent trade-off is shown in Fig. 2, where the normalized minimum stopband energy is plotted against the normalized ISI factor t_d/E_h. (In order to focus on the trade-off between the stopband energy and the ISI factor, the maximum stopband level, t_{sb}, and the maximum passband level, t_p, were chosen large enough so that these constraints were inactive.) Fig. 2 represents the inherent trade-off in the sense that no point below this curve is achievable with a length 320 filter, and points on the curve are achieved by solving (13). From this figure, it can be seen that smaller values of the stopband energy can be achieved at the price of imposing larger ISI. Smaller values of stopband energy are desirable because they result in improved subchannel isolation and hence smaller values for the power of NEXT, ICI, and echo at the receiver. On the other hand, smaller values of the ISI factor, t_d, result in less ISI. Now that we have an efficient method for computing this inherent trade-off, an important engineering design question is: At which point on this trade-off should the system operate? To provide an answer to this question, we will calculate the achievable bit rate for the system of Fig. 1. An appropriate operating point on the trade-off curve would be the one that maximizes the achievable bit rate.

The number of bits per symbol interval that can be loaded on the ith subchannel is given by [2], [4]

$$\beta_i = \log_2 \left(1 + \frac{\mathrm{SINR}_i \ \gamma_{\mathrm{code}}}{\Gamma \ \gamma_{\mathrm{margin}}} \right), \tag{14}$$

where SINR_i is the signal to noise plus interference ratio of the ith subchannel at the input to the symbol detector embedded in the detector block[2] in Fig. 1; Γ denotes the SNR gap, which for QAM modulation at a symbol error probability of 10^{-7} is about 9.8 dB [2]; γ_{code} is the coding gain; and γ_{margin} is the additional SNR margin which accounts for inaccuracies in the system model. For simplicity, we will assume that the coding gain is equal to the required additional margin in our example, i.e., $\gamma_{\mathrm{code}}/\gamma_{\mathrm{margin}} = 1$, but other values for this ratio can be easily incorporated. The achievable bit rate for assigned transmission is obtained by summing the values given by (14) over the assigned subchannels and then multiplying the result by the symbol rate $1/T$. For the downstream case we have

$$R = \frac{1}{T} \sum_{i \in \mathcal{A}} \beta_i. \tag{15}$$

We computed the achievable bit rates for the filters on the trade-off curve for a voice-grade unshielded twisted pair cable (UTP-3) model [4] for the DSL channel. Power spectral densities of NEXT and FEXT were computed based on the model for a 50-pair binder [2], [4], and the echo signal was deemed negligible compared to the other disturbances. The results were obtained for symmetric transmission with a sampling rate of 11 Msample/sec, a transmit signal power of 10 dBm, and an AWGN power spectral density equal to -140 dBm/Hz. The transmit power was uniformly distributed among all operating subchannels; i.e., no power was assigned to the subchannels that

[2]As mentioned earlier, we will focus on symbol rate decision feedback detectors in this paper.

were not capable of carrying at least one bit per symbol interval[3]. In each subchannel, symbol-spaced minimum mean square error (MMSE) decision feedback equalization was applied, with 20 taps in the feedforward section and 15 taps in the feedback section. The equalizer was assumed to be free of error propagation. (The performance obtained under this assumption resembles that obtained with the corresponding Tomlinson-Harashima precoding [18, p. 365] at the transmitter; see, e.g. [4, 19].) Fig. 3 contains a plot of the achievable bit rate against the normalized ISI factor of the prototype filter for a cable length of 1 km. It is observed that the achievable bit rate varies substantially as the designed filter traverses the trade-off in Fig. 2. For a given filter length and DFE structure, reducing the normalized ISI factor t_d/E_h reduces the impact of ISI on the achievable bit rate. However, this reduction in ISI comes at the price of an increase in the stopband energy of the prototype filter, which reflects a reduction in the subchannel spectral containment and hence an increase in the impact of ICI and NEXT on the achievable bit rate. In contrast, allowing a larger normalized ISI factor enables the designer to achieve a smaller stopband energy and hence lower levels of ICI and NEXT, at the price of increased ISI. The position of maximum achievable bit rate on the trade-off curve is dependent on the DSL environment and the structure chosen for the DFE. However, that position can be found in a straightforward manner by traversing the trade-off curve that is efficiently generated by our design method.

To explore this trend in more scenarios, achievable bit rates for cable lengths of 600, 800, 1200, 1400, and 1600 meters were also computed (for different normalized ISI factors). They are plotted together with that of 1 km cable in Fig. 4. It can be seen that while the general trend is the same, there is a slight movement of the peak when the cable length changes. For the 600-meter cable, the peak has moved to smaller values of the ISI factor, t_d, and for the 1600-meter cable the peak has shifted marginally towards larger values of the ISI factor. The movement of the peak towards larger t_d values for longer cables is because the NEXT power at the receiver is independent of the cable length, whereas the signal itself suffers from a higher level of attenuation in longer cables. Thus, the signal to NEXT power ratio at the receiver is smaller for longer cables. Consequently, longer cables require greater spectral containment; i.e., smaller stopband energy for the prototype filter. From the inherent trade-off curve in Fig. 2 it is clear that in order to provide smaller stopband energy, the prototype filter is forced to generate more ISI. Although the optimum level of spectral containment depends on the cable length, in our example it can be seen that choosing an average cable length (e.g., 1 km), and picking the optimum filter for that cable length, provides close to optimum performance for a variety of cable lengths.

[3]This is a simple power allocation scheme. While it is not optimal, in DMT systems its performance is close to that of the optimal scheme [17]. In Section 6 we will present a power allocation algorithm that is tailored to FMT.

5 Number of subchannels

In Section 4 we observed that in the FMT system there is a trade-off between ISI and the combination of ICI and crosstalk. In particular, we observed that the optimal prototype filter for the system was the one that achieved the best balance between these competing characteristics. In a similar way, the trade-off between ISI and ICI also impacts the choice of the number of subchannels. If the number of subchannels is small, the wide-bandwidth subchannels will expose the system to a high level of ISI generated by the variation of the frequency response of the channel over each band. On the other hand, as the number of subchannels grows, the spectral containment required from the prototype filter in order to keep ICI and crosstalk to a manageable level increases. According to the trade-off curve obtained in Section 4, the system will therefore suffer from an increasing amount of ISI generated by the prototype filter. As one might expect, the optimal choice for the number of subchannels requires a balance between these two sources of ISI, and in the following example we demonstrate how the tools that were developed in Sections 3 and 4 can be used to determine the appropriate number of subchannels.

We consider the FMT system in Fig. 1 in which the prototype filter had a length $L = 320$, the channel model was that in Section 4 with a cable length of 1600 meters, and the MMSE DFE in each subchannel had 20 feedforward taps and 15 feedback taps. The redundancy of the filter bank is also fixed to 12.5%, i.e., $N/M = 1.125$. By applying the design method of Sections 3 and 4 we found the optimum prototype filters (and their corresponding achievable bit rates) for a few different values of M, the number of subchannels. In order to comply with efficient structures for implementing the FMT system we chose $M = 8, 16, 32, 64$, and 128. Table 1 provides the maximum achievable bit rates versus the number of subchannels. As expected, the highest bit rate is achieved by using a moderate number of subchannels. In particular, it can be seen that for a fixed length for the prototype filter, increasing the number of subchannels does not necessarily improve the performance of the system. As stated above, this is because the high spectral containment required for large values of M can only be achieved by a prototype filter which generates a substantial amount of ISI.

6 Power loading

To compute the achievable bit rates in Section 4, a simple loading algorithm was used: the total transmit power was uniformly distributed among the subchannels that were capable of reliably transmitting at least one bit per symbol interval. Although that algorithm performs reasonably well, in this section we will present a loading algorithm that is tailored to the FMT system. We will compare the performance of this algorithm with that of the algorithm used in Section 4 and that of the conventional water-filling approach. For DMT systems it is well known [2] that water-filling provides the optimal power loading. However, as we will see below, the existence of non-negligible

ISI at the inputs to the detectors means that water-filling is not necessarily the the optimal loading method in the FMT system.

The conventional power loading problem is to maximize the achievable bit rate subject to a fixed transmit power, i.e.,

$$\text{maximize} \quad \sum_{i\in\mathcal{A}} \beta_i \tag{16a}$$

$$\text{subject to} \quad \sum_{i\in\mathcal{A}} P_i = P_{\text{total}}\,, \tag{16b}$$

$$P_i \geq 0\,, i \in \mathcal{A}, \tag{16c}$$

where β_i is given by (14) and $\mathcal{A}$ is the set of carrier indices used for communication. Recall that SINR_i in (14) is the signal to interference plus noise ratio at the input to the symbol detector embedded in the decision feedback equalizer in the detector block for the ith subchannel. Our numerical computations show that for the well-designed prototype filters (e.g., the optimum filters found in Section 4) the ICI power is negligible compared to the other noise and interferences. We emphasize that while the ICI is negligible, the ISI can be quite large and cannot be ignored. With the assumption of negligible ICI, the SINR_i can be expressed as

$$\text{SINR}_i = \frac{P_i|\tilde{f}_{ii}[d_i]|^2}{P_i \sum_{k<d_i} |\tilde{f}_{ii}[k]|^2 + P_{AWGN_i} + P_{NEXT_i} + P_{FEXT_i}} \tag{17}$$

where $\tilde{f}_{ii}[n]$ is the sequence resulting from the convolution of $f_{ii}[n]$ (which is described by (3) and (4)) with the impulse response of the feed-forward filter of the MMSE decision feedback equalizer for the ith subchannel, and d_i is the "cursor position" [18, p. 360] of the DFE. Note that we have assumed that there is no error propagation in the DFE, and hence, that the ISI from the previously detected symbols is eliminated. The terms P_{AWGN_i}, P_{NEXT_i}, and P_{FEXT_i} represent the power of the AWGN, NEXT, and FEXT components of the received signal at the output of the feed-forward filter of the DFE of the ith subchannel.

A key observation from (17) is that due to the non-negligible ISI term, both the numerator and denominator of SINR_i depend on P_i. Therefore, conventional water-filling [2] does not provide the optimum power loading. In the subsections below we will develop a power loading algorithm that explicitly incorporates the ISI. Our numerical results will show that the resulting algorithm can provide significantly higher achievable bit rates than those obtained by ignoring the ISI term and performing conventional water-filling.

6.1 Power loading algorithm

For the sake of notational simplicity, we re-write (17) as

$$\mathrm{SINR}_i = \frac{P_i a_i}{P_i b_i + c_i} \quad , \tag{18}$$

where

$$a_i = |\tilde{f}_{ii}[d_i]|^2 \,, \tag{19a}$$

$$b_i = \sum_{k<d_i} |\tilde{f}_{ii}[k]|^2 \,, \tag{19b}$$

$$c_i = P_{AWGN_i} + P_{NEXT_i} + P_{FEXT_i}. \tag{19c}$$

For a given set of feedforward filters in the DFEs, the terms a_i, b_i, and c_i are constant, and hence the numerator of SINR_i is linear in P_i and the denominator is affine. Since $\log(\cdot)$ is concave, the objective function in (16a) is a sum of concave functions and is thus concave. Furthermore, the constraints in (16b) and (16c) are linear. Therefore, for fixed a_i, b_i, and c_i the problem in (16) is convex in the allocated powers, P_is, and can be efficiently solved (using, e.g., interior point methods) to find the optimum subchannel power allocation. Once the subchannel powers are found and allocated to the FMT subchannels, the DFE coefficients have to be readjusted. When the DFE coefficients change, a_i, b_i, and c_i may change; c.f., (19). Thus, we propose the following iterative algorithm for power loading in an FMT system:

1. Starting point: Distribute the total transmit power uniformly among all the available subchannels.
2. Calculate the DFE coefficients for each subchannel.
3. Compute the power distribution by efficiently solving (16).
4. Asses progress via the two-norm of the update to the vector of power allocations and return to step 2 unless progress is negligible.

A flow diagram for this algorithm is provided in Fig. 5, where

$$\mathbf{a}^{(k)} = [a_1^{(k)}, a_3^{(k)}, \cdots, a_{M-1}^{(k)}] \,, \tag{20a}$$

$$\mathbf{b}^{(k)} = [b_1^{(k)}, b_3^{(k)}, \cdots, b_{M-1}^{(k)}] \,, \tag{20b}$$

$$\mathbf{c}^{(k)} = [c_1^{(k)}, c_3^{(k)}, \cdots, c_{M-1}^{(k)}] \,, \tag{20c}$$

$$\mathbf{p}^{(k)} = [P_1^{(k)}, P_3^{(k)}, \cdots, P_{M-1}^{(k)}] \,, \tag{20d}$$

represent the vectors of the coefficients a_i, b_i, c_i, and P_i at the kth iteration of the algorithm. An important property of this iterative algorithm is that it is guaranteed to converge. That is,

Theorem 1. *The algorithm of Fig. 5 converges.*

Proof. The proof is available in Appendix B. □

6.2 Numerical results for the loading algorithm

In this section we compare the performance of the following three loading schemes by computing the achievable bit rate for the FMT system when each of these schemes is used as the power loading method in the system. The three schemes are

1. The power loading algorithm proposed in Fig. 5;
2. Uniform distribution of the transmit power among the subchannels that are capable of carrying at least one bit information per symbol interval (this technique was used in Section 4);
3. Water-filling power loading in which the ISI component of the SINR is ignored.

Fig. 6 shows the achievable bit rates for the FMT system with each of the three loading schemes for different cable lengths of the channel model used in Section 4. For this system, the MMSE-DFE on each subchannel had 20 taps in the feedforward filter and 8 taps in the feedback filter. It can be seen from the figure that the new loading scheme offers substantially larger achievable bit rates than the other two schemes. The key factor in this rate gain is the appropriate treatment of ISI. To demonstrate this fact, in Fig. 7 we provide the numerical results for the achievable bit rates in the same environment as in Fig. 6 but with a stronger MMSE-DFE in each subchannel. This stronger DFE had 15 feedback taps rather than the 8 taps in Fig. 6. This stronger DFE provides much greater ISI suppression, and hence the difference between the achievable bit rates provided by the three loading schemes are much smaller. However, the proposed algorithm continues to provide the highest achievable bit rates. (Observe that the greater ISI suppression provided by the stronger DFE results in each loading method achieving a higher bit rate than in Fig. 6.)

Figures 6 and 7 expose a trade-off between design and implementation complexity. If the designer chooses a lower complexity receiver (i.e., fewer taps in the DFEs), then considerable achievable rate gains can be obtained by using the power loading algorithm developed in this section. On the other hand, if the designer chooses a higher complexity receiver, as we did in the examples of Sections 4 and 5, then a simple power loading algorithm will suffice.

7 Conclusion

We have addressed a number of aspects of the design of the filtered multitone communication systems. A key contribution was the development of an efficient technique for the design of the prototype filter. The design criteria were based on the measures of the intersubchannel interference (ICI) and intersymbol interference (ISI) generated by the filter bank. These criteria compete with each other and hence an effective design technique ought to enable efficient qualification of the inherent trade-off between these criteria. We were able to achieve this goal by transforming the direct formulation of the design problem into a convex optimization problem that can be efficiently solved. The resulting trade-off curves quantify the basic intuition that obtaining the optimal performance from an FMT system requires a compromise between ICI and ISI. Furthermore, they enable a designer to efficiently determine the appropriate compromise for a given scenario. As we demonstrated in our examples, the choice of an appropriate compromise between ICI and ISI offers a significant increase in the achievable bit rate. Furthermore, the availability of an efficient method for obtaining an optimal prototype filter enables quantification of other design trade-offs, such as the appropriate number of subchannels in an FMT scheme.

A characteristic of the proposed design technique is that the formulation of the design problem is independent of the detector. However, the appropriate operation point on the trade-off curve between ISI and ICI is dependent on the choice of the detector. As part of our continuing work in this area, we are developing efficiently solvable formulations of prototype design problems that will enable the designer to tailor the prototype filter design to a potential class of detectors. We expect these designs to offer a modest performance advantage over our current designs.

One of the outcomes of our prototype filter design technique is that the most effective prototype filters generate considerable ISI at the subchannel outputs. As a result, the conventional water-filling algorithm for the allocation of the transmission power to the subchannels is suboptimal. Our final contribution was the development of a convergent iterative algorithm for power loading in the FMT system. This algorithm provides higher achievable bit rates than both conventional water-filling and a simpler loading algorithm that allocates power uniformly to those subchannels that can reliably support at least one bit per subchannel use. The rate gains were shown to be significant in scenarios in which implementation constraints significantly restrict the complexity of the decision feedback equalizer in each subchannel.

Appendix

A Derivation of the upper bound for the ICI power

In this appendix, we prove that the power of ICI can be bounded as in (8). Using (3), the Fourier transform of $f_{mi}[n]$ can be written as

$$F_{mi}(e^{j\omega}) = \frac{1}{N}\sum_{k=0}^{N-1} G_{mi}(e^{j(\frac{\omega-2k\pi}{N})}), \tag{21}$$

where $G_{mi}(e^{j\omega})$ is the Fourier transform of $g_{mi}[n]$. Using (4) we have that

$$G_{mi}(e^{j\omega}) = H(e^{j(\omega-\omega_i)})H^*(e^{j(\omega-\omega_m)})C(e^{j\omega}). \tag{22}$$

Applying the triangle inequality to the magnitude of (21) we have that

$$|F_{mi}(e^{j\omega})| \leq \frac{1}{N}\sum_{k=0}^{N-1} |G_{mi}(e^{j(\frac{\omega-2k\pi}{N})})| \tag{23}$$

and using the inequality $|\sum_{i=1}^{n} a_i|^2 \leq n\sum_{i=1}^{n}|a_i|^2$ in (23) we have that

$$|F_{mi}(e^{j\omega})|^2 \leq \frac{1}{N}\sum_{k=0}^{N-1} |G_{mi}(e^{j(\frac{\omega-2k\pi}{N})})|^2. \tag{24}$$

If we let U_c denote an upper bound on the magnitude of the channel spectrum, i.e., $|C(e^{j\omega})| \leq U_c$, then from (22) and (24) we conclude that

$$|F_{mi}(e^{j\omega})|^2 \leq \frac{U_c^2}{N}\sum_{k=0}^{N-1} |H(e^{j(\frac{\omega-2k\pi}{N}-\omega_i)})H^*(e^{j(\frac{\omega-2k\pi}{N}-\omega_m)})|^2. \tag{25}$$

To calculate the bound for $\int_0^{2\pi} |F_{mi}(e^{j\omega})|^2\, d\omega$, we define the new variable $\Omega = \frac{\omega-2k\pi}{N}$, which in combination with (25) allows us to write

$$\int_0^{2\pi} |F_{mi}(e^{j\omega})|^2\, d\omega \leq U_c^2 \sum_{k=0}^{N-1} \int_{\frac{-2k\pi}{N}}^{\frac{2\pi-2k\pi}{N}} |H(e^{j(\Omega-\omega_i)})|^2 |H(e^{j(\Omega-\omega_m)})|^2\, d\Omega. \tag{26}$$

Combining the summation and the integral in (26) we obtain the bound

$$\int_0^{2\pi} |F_{mi}(e^{j\omega})|^2\, d\omega \leq U_c^2 \int_0^{2\pi} |H(e^{j(\Omega-\omega_i)})|^2 |H(e^{j(\Omega-\omega_m)})|^2\, d\Omega. \tag{27}$$

If we define P_I to be $P_I = \max_{i\in\mathcal{A}}\{P_i\}$, then using (7) and (27) we have that

$$\begin{aligned} P_{\text{ICI}} &\leq \frac{U_c^2 P_I}{2\pi} \sum_{\substack{i\in\mathcal{A}\\ i\neq m}} \int_0^{2\pi} |H(e^{j(\Omega-\omega_i)})|^2 |H(e^{j(\Omega-\omega_m)})|^2 \, d\Omega \\ &\leq \frac{U_c^2 P_I}{2\pi} \sum_{\substack{i=1\\ i\neq m}}^{M} \int_0^{2\pi} |H(e^{j(\Omega-\omega_i)})|^2 |H(e^{j(\Omega-\omega_m)})|^2 \, d\Omega. \end{aligned} \tag{28}$$

Recall that $\omega_i = (i-1)2\pi/M$. Therefore, (28) can be simplified to

$$P_{\text{ICI}} \leq \frac{U_c^2 P_I}{2\pi} \sum_{\ell=1}^{M-1} \int_0^{2\pi} |H(e^{j\omega})|^2 |H(e^{j(\omega-\ell\frac{2\pi}{M})})|^2 \, d\omega. \tag{29}$$

In order to simplify the remaining analysis, the spectral mask of the prototype filter is depicted in Fig. 8. The integral in (29) can be calculated as the integral over the passband of $H(e^{j\omega})$ plus the integral over the stopband of $H(e^{j\omega})$, i.e.,

$$\sum_{\ell=1}^{M-1} \int_0^{2\pi} |H(e^{j\omega})|^2 |H(e^{j(\omega-\ell\frac{2\pi}{M})})|^2 \, d\omega = I_1 + I_2 \,, \tag{30}$$

where

$$I_1 = \sum_{\ell=1}^{M-1} \int_{-\frac{\pi}{M}}^{\frac{\pi}{M}} |H(e^{j\omega})|^2 |H(e^{j(\omega-\ell\frac{2\pi}{M})})|^2 \, d\omega, \tag{31}$$

and

$$I_2 = \sum_{\ell=1}^{M-1} \int_{\frac{\pi}{M}}^{2\pi-\frac{\pi}{M}} |H(e^{j\omega})|^2 |H(e^{j(\omega-\ell\frac{2\pi}{M})})|^2 \, d\omega. \tag{32}$$

In the passband of the prototype filter, the spectrum is bounded by U_p. Therefore,

$$\begin{aligned} I_1 &\leq U_p^2 \sum_{\ell=1}^{M-1} \int_{-\frac{\pi}{M}}^{\frac{\pi}{M}} |H(e^{j(\omega-\ell\frac{2\pi}{M})})|^2 \, d\omega \\ &= U_p^2 \sum_{\ell=1}^{M-1} \int_{\frac{-\pi-2\pi\ell}{M}}^{\frac{\pi-2\pi\ell}{M}} |H(e^{j\omega})|^2 \, d\omega \\ &= U_p^2 \int_{-2\pi+\frac{\pi}{M}}^{-\frac{\pi}{M}} |H(e^{j\omega})|^2 \, d\omega \\ &= 2\pi \, U_p^2 \, E_{sb}, \end{aligned} \tag{33}$$

where E_{sb} is the stopband energy of the prototype filter and is given by (9). On the other hand,

the stopband magnitude of the prototype filter is bounded by U_{sb}. Thus, from (32) we have that

$$\begin{aligned} I_2 &\le U_{sb}^2 \sum_{\ell=1}^{M-1} \int_{\frac{\pi}{M}}^{2\pi-\frac{\pi}{M}} |H(e^{j(\omega-\ell\frac{2\pi}{M})})|^2 \, d\omega \\ &= U_{sb}^2 \sum_{\ell=1}^{M-1} \int_{\frac{\pi-2\pi\ell}{M}}^{2\pi-\frac{\pi+2\pi\ell}{M}} |H(e^{j\omega})|^2 \, d\omega \\ &= U_{sb}^2 \int_{-2\pi+\frac{3\pi}{M}}^{2\pi-\frac{3\pi}{M}} |H(e^{j\omega})|^2 \, d\omega \\ &\le 2\pi \, U_{sb}^2 \, (E_h + E_{sb}), \end{aligned} \tag{34}$$

where E_h is the energy of the prototype filter, $E_h = \frac{1}{2\pi}\int_0^{2\pi} |H(e^{j\omega})|^2 \, d\omega$. The last inequality in bounding I_2 (in (34)) can be simply verified using Fig. 8.

Finally, using (29), (30), (33), and (34) we conclude that

$$P_{\text{ICI}} \le P_I U_c^2 (U_p^2 E_{sb} + U_{sb}^2 E_h + U_{sb}^2 E_{sb}). \tag{35}$$

B Proof of theorem 1

Refer to the flow diagram of the power loading algorithm given in Fig. 5. When the kth iteration of the algorithm begins, the subchannel powers are given by the vector $\mathbf{p}^{(k)}$. Once the MMSE-DFE coefficients are adjusted for the given $\mathbf{p}^{(k)}$, the achievable bit rate of the system can be calculated as a function of $\mathbf{a}^{(k)}, \mathbf{b}^{(k)}, \mathbf{c}^{(k)}$ and $\mathbf{p}^{(k)}$ using (15). We denote this rate as $R(\mathbf{a}^{(k)}, \mathbf{b}^{(k)}, \mathbf{c}^{(k)}, \mathbf{p}^{(k)})$. In the next stage of the algorithm, for the given $\mathbf{a}^{(k)}, \mathbf{b}^{(k)}, \mathbf{c}^{(k)}$ the optimization problem (16) is solved which results in $\mathbf{p}^{(k+1)}$. Obviously,

$$R(\mathbf{a}^{(k)}, \mathbf{b}^{(k)}, \mathbf{c}^{(k)}, \mathbf{p}^{(k+1)}) \ge R(\mathbf{a}^{(k)}, \mathbf{b}^{(k)}, \mathbf{c}^{(k)}, \mathbf{p}^{(k)}). \tag{36}$$

In the next iteration, the MMSE-DFE coefficients are calculated for the new power allocation vector $\mathbf{p}^{(k+1)}$, resulting in $\mathbf{a}^{(k+1)}, \mathbf{b}^{(k+1)}, \mathbf{c}^{(k+1)}$. Since the adjustment of the MMSE-DFE coefficients for the new power vector $\mathbf{p}^{(k+1)}$ results in an improvement in the SINR of the subchannels, we obtain an increase in the achievable bit rate. More precisely,

$$R(\mathbf{a}^{(k+1)}, \mathbf{b}^{(k+1)}, \mathbf{c}^{(k+1)}, \mathbf{p}^{(k+1)}) \ge R(\mathbf{a}^{(k)}, \mathbf{b}^{(k)}, \mathbf{c}^{(k)}, \mathbf{p}^{(k+1)}). \tag{37}$$

Equations (36) and (37) show that the achievable bit rate of the system increases monotonically. On the other hand, we know that the achievable bit rate of the system is bounded above, say by the capacity of the system. Thus, the algorithm converges.

References

[1] T. Starr, M. Sorbara, J. M. Cioffi, and P. J. Silverman, *DSL Advances*, Prentice-Hall, 2003.

[2] T. Starr, J. M. Cioffi, and P. J. Silverman, *Understanding Digital Subscriber Line Technology*, Prentice-Hall, 1999.

[3] D. Mestdagh, M. Isaksson, and P. Ödling, "Zipper VDSL: A Solution for Robust Duplex Communication over Telephone Lines," *IEEE Commun. Mag.*, vol. 38, pp. 90-96, May 2000.

[4] G. Cherubini, E. Eleftheriou, and S. Ölçer, "Filtered Multitone Modulation for Very High-Speed Digital Subscriber Lines," *IEEE J. Select. Areas Commun.*, vol. 20, pp. 1016-1028, June 2002.

[5] G. Cherubini, E. Eleftheriou, S. Ölçer, and J. Cioffi, "Filter Bank Modulation Techniques for Very High-Speed Digital Subscriber Lines," *IEEE Commun. Mag.*, vol. 38, pp. 98-104, May 2000.

[6] S. Mirabbasi, and K. Martin, "Oversampled Complex-Modulated Transmultiplexer Filters with Simplified Design and Superior Stopbands," *IEEE Trans. Circuits Syst. II*, vol. 50, pp. 456-469, Aug. 2003.

[7] S. M. Phoong, Y. Chang, and C. Y. Chen, "SIR-optimized DFT-bank transceivers for multipath fading channels," in *Proc. IEEE Int. Conf. Acoust., Speech, and Sig. Proc.*, vol. 4, pp. 729-732, May 2004.

[8] G. Cherubini, "Hybrid TDMA/CDMA based on filtered multitone modulation for uplink transmission in HFC networks," *IEEE Commun. Mag.*, vol. 41, pp. 108-115, Oct. 2003.

[9] N. Benvenuto, S. Tomasin, and L. Tomba, "Equalization methods in OFDM and FMT systems for broadband wireless communications," *IEEE Trans. Commun.*, vol. 50, pp. 1413-1418, Sept. 2002.

[10] L. Vandendorpe, L. Cuvelier, F. Deryck, J. Louveaux, and O. van de Wiel, "Fractionally spaced linear and decision-feedback detectors for transmultiplexers," *IEEE Trans. Signal Processing*, vol. 46, pp. 996-1011, Apr. 1998.

[11] P. P. Vaidyanathan, *Multirate Systems and Filter Banks*, Prentice-Hall, 1993.

[12] M. R. Wilbur, T. N. Davidson, and J. P. Reilly, "Efficient design of oversampled NPR GDFT filter banks," *IEEE Trans. Signal Processing*, vol. 52, pp. 1947-1963, July 2004.

[13] T. N. Davidson, Z. Q. Luo, J. F. Sturm, "Linear matrix inequality formulation of spectral mask constraints with applications to FIR filter design," *IEEE Trans. Signal Processing*, vol. 50, pp. 2702-2715, Nov. 2002.

[14] J.F. Sturm, "Using SeDuMi 1.02, a MATLAB toolbox for optimization over symmetric cones", *Optimiz. Methods Softw.*, vol. 11-12, pp. 625-653, 1999.

[15] S. P. Wu, S. Boyd, and L. Vandenberghe, "FIR filter design via spectral factorization and convex optimization," in *Applied and Computational Control, Signals, and Circuits*, vol. 1, B. Datta, Ed., Birkhauser, 1997.

[16] T. N. T. Goodman, C. A. Micchelli, G. Rodriguez, and S. Seatzu, "Spectral factorization of Laurent polynomials," *Adv. Comput. Math.,* vol. 7, No. 4, pp.429-454, 1997.

[17] W. Yu, and J. M. Cioffi, "On constant power water-filling," in *Proc. IEEE Int. Conf. Commun.*, vol. 6, pp. 1665-1669, Helsinki, June 2001.

[18] J. R. Barry, E. A. Lee, and D. G. Messerschmitt, *Digital Communication*, 3rd Edition, Kluwer, 2004.

[19] N. Benvenuto, and S. Tomasin, "Efficient pre-coding schemes for FMT broadband wireless systems," in *Proc. IEEE Int. Symp. Personal, Indoor, Mobile Radio Commun.*, vol. 4, pp. 1493-1497, Lisbon, Sept. 2002.

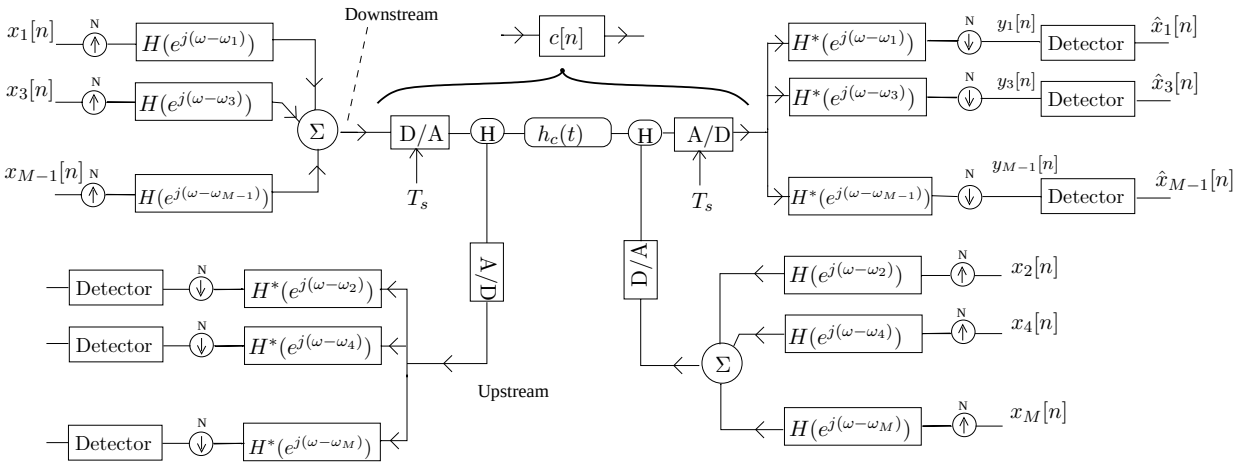

Figure 1: An M-channel filtered multitone (FMT) communication system. We will focus on systems in which the detector incorporates a decision feedback equalizer (DFE).

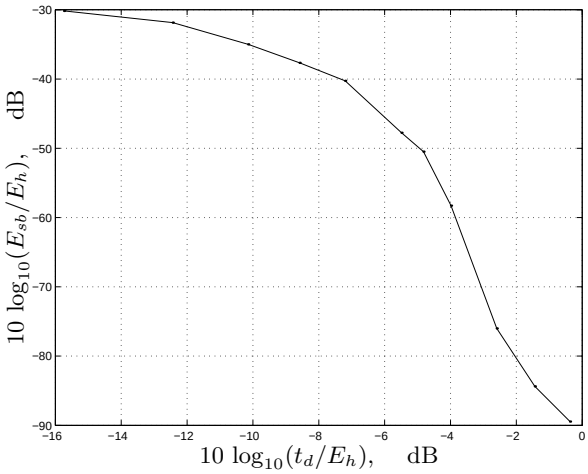

Figure 2: Trade-off curve for the normalized stopband energy against the normalized ISI factor of the prototype filter for an FMT system with $M = 32$ subchannels, up/down sampling factor $N = 36$, and a prototype filter of length 320.

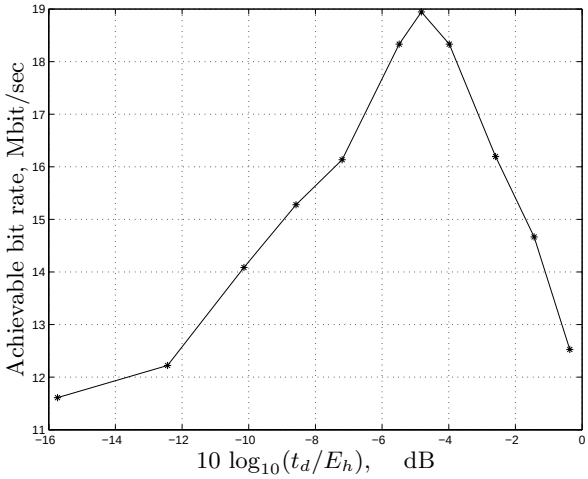

Figure 3: Achievable bit rate versus normalized ISI factor of the prototype filter for an FMT system with $M = 32$ subchannels, up/down sampling factor $N = 36$, a prototype filter of length 320, a sampling rate of 11 Msample/sec, and a cable length of 1 km.

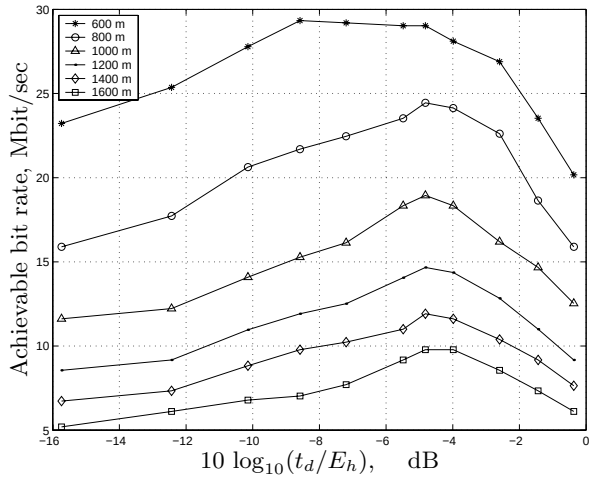

Figure 4: Achievable bit rate versus normalized ISI factor of the prototype filter for different cable lengths. The FMT system has the characteristics of $M = 32$ subchannels, up/down sampling factor $N = 36$, a prototype filter of length 320, and a sampling rate of 11 Msample/sec.

Table 1: Maximum achievable bit rate versus the number of subchannels for a cable length of 1600 meters.

M	N	Maximum achievable bit rate Mbit/sec
8	9	2.07
16	18	4.89
32	36	10.33
64	72	8.96
128	144	3.68

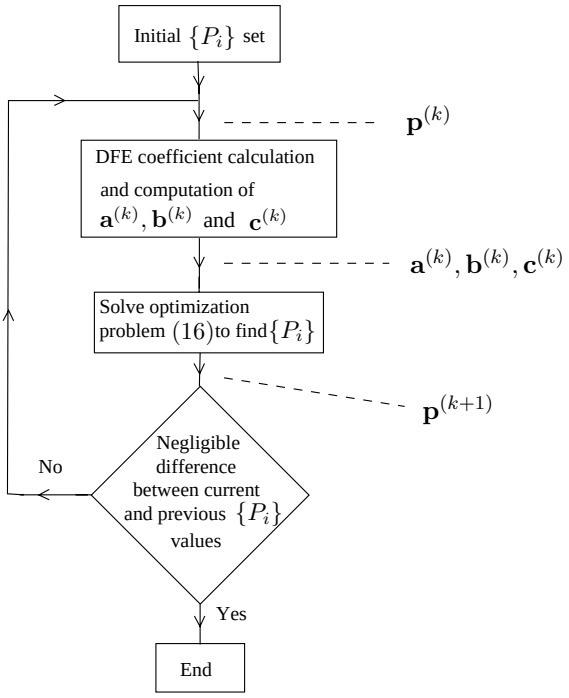

Figure 5: The proposed power loading algorithm for the FMT system.

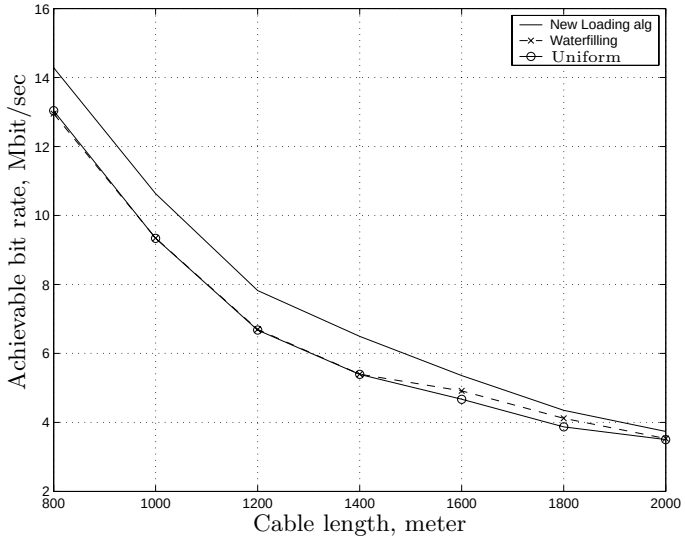

Figure 6: Achievable bit rate versus cable length for the three loading schemes. The FMT system had the following characteristics: $M = 32$, $N = 36$, prototype filter of length $L = 320$, and a sampling rate of 11 Msample/sec. DFE for the subchannels had 20 taps in the feedforward section and 8 taps in the feedback section.

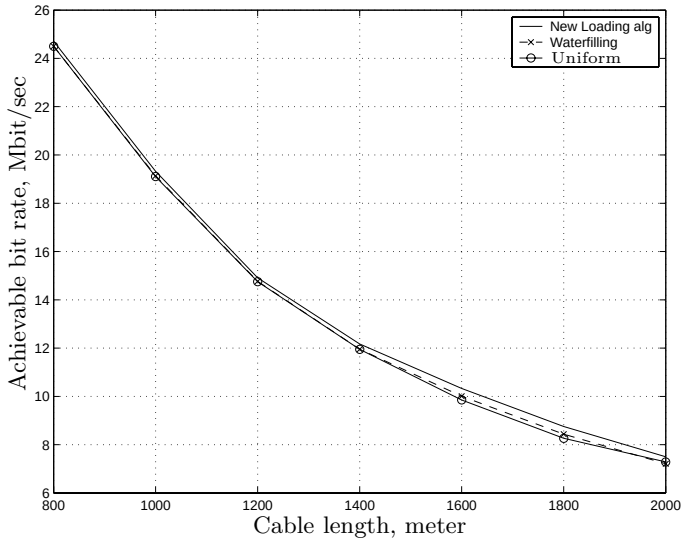

Figure 7: Achievable bit rate versus cable length for the three loading schemes. The FMT system had the following characteristics: $M = 32$, $N = 36$, prototype filter of length $L = 320$, and a sampling rate of 11 Msample/sec. DFE for the subchannels had 20 taps in the feedforward section and 15 taps in the feedback section.

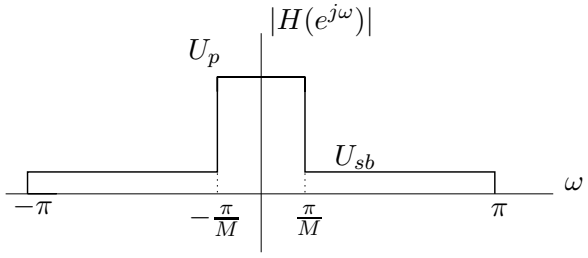

Figure 8: Prototype filter spectrum mask.